ELSEVIER

Photovoltage effects in photoemission from thin GaAs layers

G.A. Mulhollan [a,1], A.V. Subashiev [a,2], J.E. Clendenin [a], E.L. Garwin [a], R.E. Kirby [a], T. Maruyama [a], R. Prepost [b,*]

[a] *Stanford Linear Accelerator Center, Stanford, CA 94309, USA*
[b] *Department of Physics, University of Wisconsin, Madison, WI 53706, USA*

Abstract

A set of thin GaAs *p*-type negative electron affinity (NEA) photocathodes have been used to measure the yield of photoemitted electrons at high intensity excitation. The active layer thickness is 100 nm and the *p*-type doping ranges from 5×10^{18} to 5×10^{19} cm^{-3} for a set of four samples. The results show that the surface escape probability is a linear function of the NEA energy. The surface photovoltage effect on photoemission is found to diminish to zero at a doping level of 5×10^{19} cm^{-3}. The experimental results are shown to be in good agreement with calculations using a charge limit model based on surface photovoltage kinetics that assume a constant electron energy relaxation rate in the band bending region. © 2001 Elsevier Science B.V. All rights reserved.

PACS: 29.25.Bx; 73.50.Pz; 73.61.Ey; 79.60.-i; 85.60.H

1. Introduction

The negative electron affinity (NEA) state of activated (100) GaAs has been widely studied and used for a variety of applications. While the qualitative features of the electron photoemission are known, a full quantitative understanding is lacking [1,2]. The coadsorption of Cs and O (or F) on an atomically clean surface of *p*-type GaAs is known to result in a significant lowering of the GaAs electron affinity as well as a shift of the surface Fermi level deep into the band gap

with a formation of the band bending region (BBR) near the surface. The band-bending is an important contribution to the lowering of the electron affinity. The emitted electron energy distribution depends on the density of states, the doping level and the electron kinetics in the BBR, leading to differing interpretations of the electron energy distribution (EDC) curves [3–6]. While the activated surface develops a surface barrier for the electrons, the structure and transparency of the barrier is not well understood.

Information on the properties of the NEA surface is obtained with photoemission studies at high power excitation [7–9]. When the photocathode is excited with high densities of light near the band gap, the total photoemitted charge is not proportional to the light intensity. This phenomenon was first observed using bulk GaAs [8], and can be described as a surface charge limit (SCL). Several experimental studies have

---

* Corresponding author.
E-mail address: prepost@hep.physics.wisc.edu (R. Prepost).
[1] Present address: Extreme Devices Inc., Austin, TX 78701, USA.
[2] Permanent address: St. Petersburg State Technical University, 195251 St. Petersburg, Russia.

been made on strained GaAs [7], superlattice structures [10], and thin unstrained GaAs [11]. In [12] the SCL was attributed to the photovoltage building up in the band bending region. The photoelectrons captured in the BBR produce an opposing field that flattens the bands and reduces NEA, which can be described as the effect of the surface photovoltage (SPV). It was determined that SPV formation and its relaxation is mainly controlled by the restoring current of the holes [13] and is very sensitive to the transparency of the barrier for the holes formed by the BBR [14]. The value of the surface photovoltage at several temperatures for a (100) GaAs surface has been measured in studies of core-level photoemission spectra under synchrotron radiation excitation [14] and in studies of the EDC at high excitation levels [11].

The problem of the SCL is important for operation of polarized electron photocathodes at the Stanford linear collider (SLC) [15] and even more so for the next generation linear colliders such as the next linear collider (NLC) [16]. The present NLC design requires a train of 95 microbunches spaced 2.8 ns apart. Each microbunch is required to have 2.8×10^{10} electrons with a peak current of 4.5 A, totaling 2.7×10^{12} electrons in a 266 ns train. The required total charge is two orders of magnitude higher than the SLC case.

In the present Letter, we report on the first detailed experimental studies and theoretical analysis for a set of 100-nm-thick GaAs samples with various levels of uniform doping. For thin-layer cathodes the time of electron extraction from the active layer to the BBR is much smaller than the bulk lifetime and the diffusion time, eliminating the influence of the recombination effects in the layer. The optical properties of unstrained GaAs are fairly well known, allowing reliable estimation of the surface escape probability from the experimental data. Using long-pulse excitation and pump–probe measurements, the kinetics of photovoltage buildup and electron emission are investigated.

2. The charge limit model

2.1. Surface escape probability

Fig. 1 shows schematically the GaAs band structure near the surface activated by Cs(O/F) deposition and the electron potential near the surface. When the
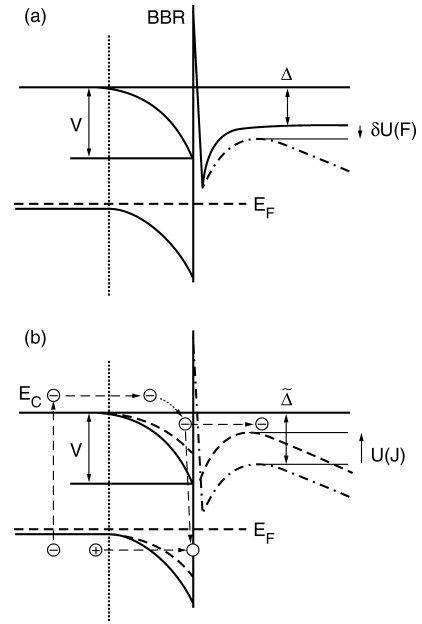

Fig. 1. Energy band diagram of a GaAs active layer showing the negative electron affinity vacuum level for various conditions. (a) The NEA variation with the bias field $\delta U(F)$ and (b) the photovoltage $U(J)$ with the arrows indicating the direction of the movement of the NEA level. The photoemission and hole recombination processes are shown schematically in part (b).

cathode is illuminated with a pulsed laser with photon energy slightly above the band gap energy, the photoexcited electrons in the conduction band are rapidly thermalized and captured in the BBR potential well from which they tunnel into vacuum through the surface barrier. For a thin unstrained GaAs layer ($\alpha d \ll 1$, $\alpha L \ll 1$, where α is the optical absorption coefficient, d is the active layer thickness, L is the diffusion length) all the electrons optically excited in the GaAs layer near the absorption edge are captured in the BBR region forming the flow of the electrons to the surface, $j_{el} = q\alpha d(1 - R)J$, where J is the light excitation intensity and R is the surface optical reflection coefficient. A part of this flow is emitted into vacuum, while the rest contributes to the surface recombination current, so that the quantum yield Y is [2]

$$Y = \alpha d(1 - R)B_N. \tag{1}$$

Here B_N is the surface escape probability. The value of B_N depends on the details of the competition between

electron recombination in the BBR and emission into vacuum through the surface barrier.

To estimate local values of B_N on the activated surface we use the results of near band gap low-intensity measurements of the quantum yield for a small excitation spot. Taking $d = 10^{-5}$ cm, $1 - R = 0.68$ and $\alpha = 5 \times 10^3$ cm^{-1} [17], we obtain $B_N \approx 0.15$ for a typical quantum yield of a thin GaAs layer of $Y = 0.5\%$. Thus, even at the low-intensity excitation only $(1/7)$th of the electron flow to the surface is photoemitted into vacuum, and the majority recombines in the band bending region.

The quantum yield from NEA surfaces increases with bias field at the GaAs surface [18,19]. This effect is attributed traditionally to the image-force lowering of the surface barrier by the applied field (see Fig. 1(a)). This barrier lowering, δU, can be evaluated from a simple electrostatic consideration:

$$\delta U(F) = q\sqrt{\frac{qF(\epsilon_s - 1)}{4\pi\epsilon_0(\epsilon_s + 1)}}, \qquad (2)$$

where q is the free electron charge, F is the external electric field, and ϵ_s is the relative permittivity of the semiconductor. The quantity $\delta U(F)$ is seen to be proportional to the square root of the bias field. More commonly, this effect is studied for surfaces having positive electron affinity or Schottky barriers, where the image force modifies the thermionic emission current. The emission current is then an exponential function of the barrier height, so that $\log(Y)$ grows linearly with the square root of applied bias field. For NEA photocathodes, both linear [19] and logarithmic [7] dependences of Y on the square root of the bias field have been observed. In Appendix A an expression for the surface escape probability B_N is derived. For the conditions of this experiment the dependence of B_N on the NEA value Δ is shown to be linear. From these considerations it follows that the relative variation of the yield with the bias field F is given by

$$\frac{Y(F)}{Y(0)} = 1 + \frac{\delta U(F)}{\Delta}. \qquad (3)$$

2.2. The photovoltage

Under intense optical excitation the electron flow to the surface starts to compensate the positive charge of the donor-like states that provide band bending at the surface. This results in a flattening of the energy bands and a lifting of the bottom of the conduction band at the surface (see the dashed curve in Fig. 1(b)). One can assume that the properties of the resulting effective surface barrier in the several monolayer-thick activation layer are not influenced by this relatively small shift. One can further assume that the electron diffusion to the band bending region does not change since it remains faster than the surface processes. The change in quantum yield can then be evaluated if one replaces the NEA value Δ by $\Delta - U(J)$, where $U(J)$ is the up-shifting of the conduction band due to the photovoltage. Taking into account the bias field effect, we obtain

$$\frac{Y(J)}{Y_0} = 1 - \frac{U(J)}{\tilde{\Delta}}, \qquad (4)$$

where $\tilde{\Delta} = \Delta + \delta U$ is the NEA value recalculated for a given bias field, δU is the potential barrier lowering resulting from an external bias field, and Y_0 is the quantum yield for non-charge-limited photoemission.

2.3. The restoring currents

When the excited electrons are captured in the BBR, the majority of electrons recombine at the surface with the holes coming from the valence band. There are several mechanisms for electron recombination (starting from the recombination in the band bending region itself). However, for activated GaAs surfaces the electron capture by surface localized states appears to be the fastest process since the electrons drift in the strong electric field to these capture centers, which have an attractive Coulomb potential. Therefore the recombination rate of these electrons is limited by the excess hole current to the surface, j_p. In the stationary state where the excitation time is much longer than the surface process time, the SPV value can be evaluated from the balance of the surface current densities, $j_{\text{el}} = j_p$.

There are two major mechanisms providing the re-combination hole current to the surface through the band bending region: thermionic emission and tunneling through the barrier. The photovoltage dependence of the hole current at low temperatures tracks with the tunneling contribution, while at higher temperatures the hole current increases due to the thermal shift of the hole energy distribution, which assists hole tunnel-

ing through the barrier. In the equilibrium state with no illumination, the excess hole current equals zero at the equilibrium band bending. Therefore, the resulting excess current $j_p(U)$ can be expressed as [20]

$$j_p(U) = j_{p,0}\left[\exp(U/E_0) - 1\right], \quad (5)$$

where the energy E_0 for the band bending region is given by

$$E_0 = E_{00} \coth\left(\frac{E_{00}}{kT}\right),$$

$$E_{00} = \frac{\hbar}{2}\left[\frac{q^2 N_a}{m_h \epsilon_0 \epsilon_s}\right]^{1/2} = 18.57\left[\frac{N_a}{m_h \epsilon_s}\right]^{1/2} \text{ meV}, \quad (6)$$

where m_h is the hole mass, and N_a is the acceptor concentration in the unit of 10^{18} cm^{-3}. For the case of thermally assisted tunneling in metal–semiconductor junctions, $j_{p,0}$ can be expressed as

$$j_{p,0} = A^{**}\frac{T(E_{00}V)^{1/2}}{k\cosh(E_{00}/kT)}\exp\left(-\frac{V}{E_0}\right), \quad (7)$$

where k is the Boltzmann constant and A^{**} is the effective Richardson constant, $A^{**} = 9.6$ A K^{-2} cm^{-2}, for tunneling by light holes. It follows from Eq. (6) that for GaAs and a typical doping level of 5×10^{18} cm^{-3}, the value of E_{00} can vary from 17 to 40 meV depending on the relative contribution of the light and heavy holes into the hole current. However, the light hole contribution to $j_p(U)$ is dominant due to the mass dependence of the $j_{p,0}$ factor. The above expression for $j_{p,0}$ is in the context of a Schottky barrier model with a metallic layer and thus may be different for cesiated NEA GaAs surfaces.

3. Experiment

The samples for the present experiment were grown by the Quantum Epitaxial Devices Corporation [21] using molecular-beam-epitaxy (MBE). The substrate material was (100) n-type (Si doped to 1×10^{18} cm^{-3}) GaAs. Since heavy p-type doping is necessary to achieve a NEA surface, a 0.1-μm-thick p-type GaAs (Be doped to 5×10^{18} cm^{-3}) layer was first grown on the substrate, followed by a 1-μm-thick p-type (Be doped to 5×10^{18} cm^{-3}) Al$_{0.3}$Ga$_{0.7}$As buffer layer. The 0.1-μm-thick p-type GaAs active layer was then grown on this buffer. Four samples were grown with uniform doping concentrations of 5×10^{18}, 1×10^{19}, 2×10^{19}, and 5×10^{19} cm^{-3} in the active layer respectively. The Al$_{0.3}$Ga$_{0.7}$As intermediate layer serves as a potential barrier to isolate the active GaAs layer from the substrate GaAs. In order to preserve an atomically clean surface the samples were anodized to form an oxide layer of about 50 Å on the GaAs surface [22]. The oxide layer was later removed as described below. The relevant sample parameters are tabulated in Table 1.

The experiments were performed at the Gun Test Laboratory at SLAC [15]. The apparatus, which is a replica of the first few meters of the SLAC injector beamline, consists of a 22.5 mm diameter photocathode diode gun with a load-lock system for cathode loading/removal, and an electron beamline terminating into a Faraday cup. Prior to installation in the system, the sample was degreased in a boiling solution of trichloroethane. After the protective oxide layer

Table 1
The parameters of differently doped GaAs cathode layers as determined from the high intensity excitation experimental data

	Sample					
	1a	1b	2a	2b	3	4
p (10^{19} cm^{-3})	0.5	0.5	1	1	2	5
$\langle Y \rangle$ (%)	0.6	0.45	0.9	0.3	0.4	0.4
τ (ns)	160	130	78	63	6	<4
E_0 (meV)	45	46	58	66	–	–
$j_{p,0}/q$ (10^{18} cm^{-2} s^{-1})	1.3	1.2	3.1	3.8	–	–

Here $\langle Y \rangle$ is the surface averaged quantum yield as determined from low bias voltage measurements. Samples 1a, 1b and 2a, 2b are different activations for samples 1 and 2, respectively.

was removed in ammonium hydroxide, the sample was rinsed in distilled water and methanol. The load-lock system was essential for loading the samples into and removing them from the gun under vacuum. This system avoided the cathode contamination that normally accompanies the bake of the gun system, resulting in reproducible cathode activations and high quantum yield. The cathode activation to obtain an NEA surface consisted of heat cleaning to 600°C for 1 h, followed by application of cesium until the photoyield peaked, and then cesium and nitrogen-trifluoride codeposition until the photoyield was again maximized.

Two different excitation sources were used for the two types of measurements. The first type of measurement used a flash-lamp pumped Ti:sapphire laser (Flash-Ti) producing a long laser pulse adjustable from 150–350 ns at 120 Hz with energy up to 130 μJ. This excitation mode was used to directly study the time evolution of the photovoltage and the dependence of the photovoltage on the laser intensity. The second type of measurement used two pulsed Ti:sapphire lasers pumped by a single frequency-doubled Nd:YAG laser (YAG-Ti) in a pump-pulse/probe-pulse combination. In this excitation mode the pump-pulse was an intense short pulse inducing a photovoltage in the photocathode followed by a short high intensity probe-pulse, but not in the intensity regime to produce a photovoltage effect. The two YAG-Ti lasers each produced a 2 ns pulse at 60 Hz with a pump laser energy of up to 100 μJ. In these measurements, the time separation between the pump and probe laser pulses was varied. This technique allowed an independent measurement of the photovoltage parameters. All laser wavelengths were 850 nm, and the spot size was set to about 20 mm so as to fill the exposed area of the cathode.

An optically isolated nanoammeter, a beam position monitor (BPM), a ceramic gap monitor, and a fast Faraday cup were used for beam intensity measurements. The cathode was biased at −120 kV and maintained at a temperature of 0 ± 2°C. The vacuum in the gun was maintained at about 1×10^{-11} Torr by means of ion and non-evaporative getter pumping.

Two low-power CW diode lasers of 833 and 850 nm were used for the low power quantum yield measurements. For an individual sample, the quantum yield typically varied by a factor of two over the surface, but in some cases as high as a factor five. These variations were presumably caused by the inhomogeneous dis-

tribution of cesium on the surface. Similar variations were reported in Ref. [19]. The quantum yield values averaged over the surface for the individual samples are shown in Table 1.

4. Results

The bias field dependence of the quantum yield was measured using the low power 833 nm diode laser. Fig. 2 shows the experimentally observed variation of the quantum yield with the bias field for sample 1a, sample 3, and two other photocathodes not used for the present experiment. These two additional samples were zinc-doped strained GaAs and carbon-doped 1 μm thick GaAs. The observed dependence clearly favors a linear rather than a logarithmic dependence of Y on $\sqrt{F}$. Following Eq. (3), the zero-field NEA value Δ can be determined from the slope of the fitted curves, shown as a solid line in Fig. 2, giving values of Δ in the range $\Delta = 122 - 138$ meV. These NEA values are, to a good approximation, the same for all well activated samples. As a comparison, the values extracted from the data of Ref. [19] for different points on the surface of a thick GaAs cathode are in the range of $100 - 160$ meV. Therefore the quality of the activation in both cases is found to be similar.

The surface charge limit effect can be explored if the cathode is excited with a high peak power laser using a pulse length much longer than the charac-
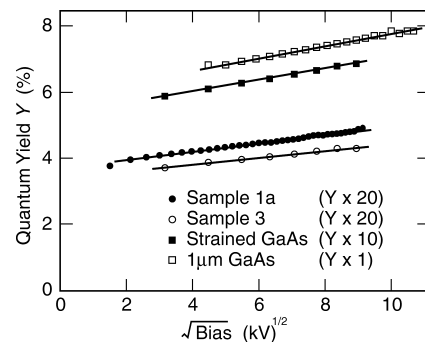

Fig. 2. The bias field dependence of the quantum yield for various photocathodes. Solid circles: sample 1a; open circles: sample 3; solid squares: zinc-doped strained GaAs; open squares: carbon-doped 1-μm-thick GaAs. The quantum yields have been rescaled as indicated in the figure.
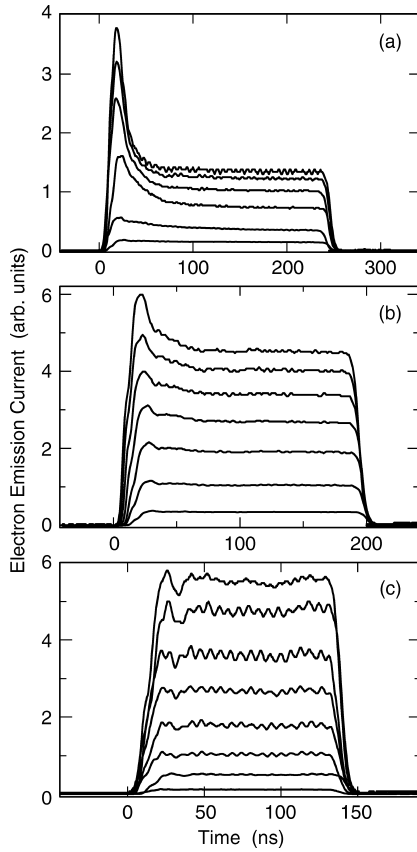
Fig. 3. The temporal profiles of the electron emission current using a long laser excitation pulse for (a) sample 1b, (b) sample 2a, and (c) sample 3. The laser intensity is varied from 1 to 150 W/cm^2.

teristic time scale of the surface photovoltage effect. This is the technique using the long-pulse Flash-Ti laser described earlier. Figs. 3(a), (b), and (c) show representative temporal profiles of the emission current pulses measured using varying light pulse energies for (a) sample 1b, (b) sample 2a, and (c) sample 3, respectively. The observed photovoltage effect has several features. As seen in Fig. 3(a), the electron emission current rises to a peak at the start of the laser pulse and then decreases as the photovoltage builds up. With time the electron emission current reaches a steady state value as the photovoltage saturates. With increasing laser energy, the photovoltage builds up more quickly and the suppression of the emission current due to the photovoltage is more pronounced. Figs. 3(b) and (c) show that the

photovoltage effect decreases as the doping level increases.

To understand the temporal profile of the emission current, the charge limit model described in Section 2 is used. The time variation of the excess electronic charge Q at the surface can be written in terms of the capacitance per unit surface area and the restoring hole current as

$$C\frac{dU}{q\,dt} = j_{el} - j_p(U) = q\alpha d(1-R)J - j_p(U). \quad (8)$$

Within the depletion region approximation [20] for the BBR region with width w, the capacitance is given by

$$C = \epsilon_0\epsilon_s/w = \sqrt{\frac{q^2\epsilon_s\epsilon_0 N_a}{2(V-U)}}, \quad (9)$$

where V is the initial band bending energy (see Fig. 1). Here we assume that the emission current is much smaller than the recombination current since the surface escape probability $B_N \approx 0.15$. Integration of Eq. (8) using Eq. (5) gives for the normalized yield:

$$\frac{Y(J)}{Y_0} = 1 + \frac{E_0}{\tilde{\Delta}}$$
$$\times \ln\left[\frac{1 + qJ/\tilde{j}_{p,0}\exp[-(1+qJ/\tilde{j}_{p,0})t/\tau]}{(1+qJ/\tilde{j}_{p,0})}\right], \quad (10)$$

where $\tilde{j}_{p,0} = j_{p,0}/\alpha d(1-R)$ and $\tau = E_0 C/q j_{p,0}$. The quantum yield decreases with a characteristic saturation time constant τ', where

$$\tau' = \frac{\tau}{(1+qJ/\tilde{j}_{p,0})}, \quad (11)$$

and reaches the steady state value:

$$Y(J)/Y_0 = 1 - \frac{E_0}{\tilde{\Delta}}\ln\left(1 + \frac{qJ}{\tilde{j}_{p,0}}\right). \quad (12)$$

Figs. 4(a), (b), and (c) show the measured dependencies of the steady state emission current on the light excitation intensity for samples 1a and 1b (Fig. 4(a)), samples 2a and 2b (Fig. 4(b)), and sample 3 (Fig. 4(c)), respectively, measured for a broad range of excitation intensities. The solid lines in Fig. 4 are fits for $JY(J)$ using Eq. (12). The SCL effect appears as the deviation of the emission current from a linear dependence on the excitation light intensity and is more pronounced in the lower doped samples (samples 1a and
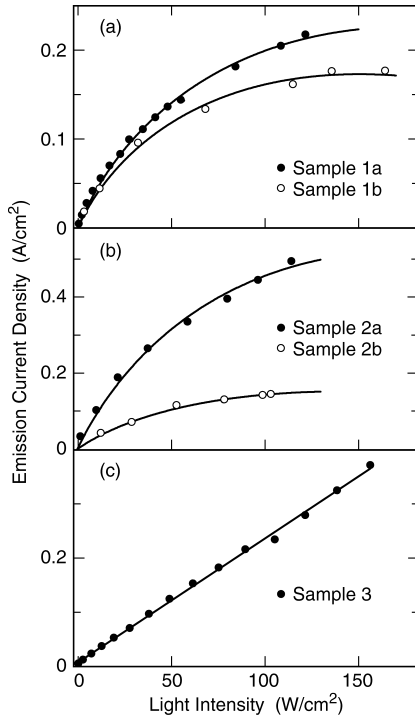
Fig. 4. The steady state emission current as a function of the light excitation intensity for (a) samples 1a and 1b, (b) samples 2a and 2b, and (c) sample 3. The solid lines are fitted results to Eq. (12).
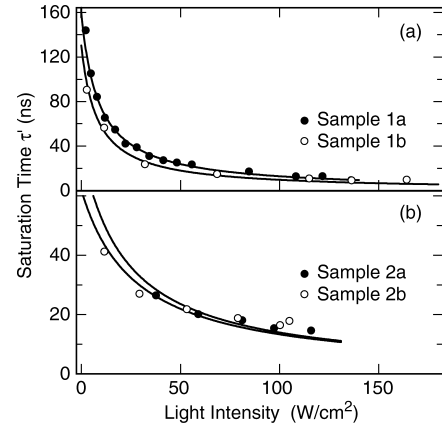

Fig. 5. The saturation time constant τ' of the photovoltage as a function of excitation light intensity for (a) samples 1a and 1b, and (b) samples 2a and 2b. The solid lines are fitted results to Eq. (11).

1b). The SCL effects are not observed in the samples with $p = 2 \times 10^{19}$ cm^{-3} (sample 3) and 5×10^{19} cm^{-3} (sample 4, not shown in Fig. 4).

Figs. 5(a) and (b) show the experimentally observed variation of the saturation time τ' as a function of the excitation intensity for (a) samples 1a, 1b, and (b) samples 2a, 2b. The saturation time shortens as the excitation intensity is increased, consistent with Eq. (11). The solid lines in Fig. 5 represent the results of a fit to Eq. (11).

The decay of the surface photovoltage can also be explored using the pump–probe technique described earlier. The short intense pump laser pulse induces a photovoltage which subsequently decays in time according to

$$C \frac{dU}{q\,dt} = -j_p(U). \tag{13}$$

The solution of Eq. (13) (neglecting the weak variation of the BBR capacitance with illumination) gives

$$U(t) = -E_0$$
$$\times \ln\left[1 - \left(1 - \exp\left(-\frac{U(0)}{E_0}\right)\right)\exp\left(-\frac{t}{\tau}\right)\right]. \tag{14}$$

Here it is seen that τ, from Eq. (10), is the characteristic relaxation time of the photovoltage. The photocathode is then illuminated by the second short laser pulse at time t at which time the photovoltage is $U(t)$. Using Eq. (4), the expression for the quantum yield $Y(t)$ of the probe pulse relative to the yield with no photovoltage effect is then given by

$$\frac{Y(t)}{Y_0} = 1 + \frac{E_0}{\tilde{\Delta}}$$
$$\times \ln\left[1 - \left(1 - \exp\left(-\frac{U(0)}{E_0}\right)\right)\exp\left(-\frac{t}{\tau}\right)\right]. \tag{15}$$

Fig. 6 shows the time variation of this ratio for samples 1b, 2a, 2b, and 3. At large times t it is seen that the photovoltage has decayed and the yield ratio asymptotically approaches one. The solid lines in Fig. 6 are the results of a fit to Eq. (15).

The data of Fig. 2 for $Y(F)$ vs. $\sqrt{F}$ are used to determine the quantity $\delta U(F)/\Delta$ using Eqs. (2) and (3). With $\delta U = 47$ meV for a bias voltage of -120 kV, the average zero-field NEA value is determined to be $\Delta = 133$ meV ($\tilde{\Delta} = \Delta + \delta U = 180$ meV). The data of Fig. 4 for $JY(J)$ vs. J are used to determine the
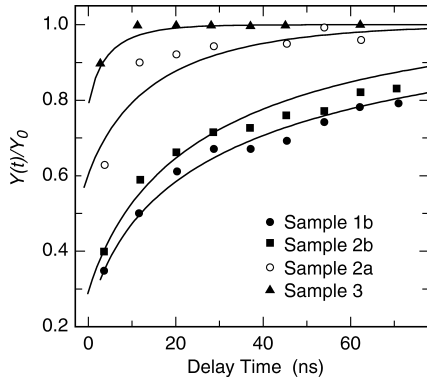
Fig. 6. The quantum yield as a function of delay time between the pump and probe pulses from pump–probe measurements for samples 1b, 2a, 2b, and 3. The solid lines are fitted results to Eq. (15).

quantities $E_0/\tilde{\Delta}$ and $j_{p,0}$ using Eq. (12) from which the parameter E_0 is calculated. The data of Fig. 5 for τ' vs. J are used to determine the quantity τ and independently determine $j_{p,0}$ using Eq. (11). Finally, the pump–probe data of Fig. 6 are used as an independent method to determine the relaxation time τ using Eq. (15). The average values of these parameters resulting from the fits are tabulated in Table 1.

5. Discussion

The most important and theoretically predictable parameter is E_0. The fit procedure yields $E_0 = 45$ meV for the average of samples 1a and 1b, and 62 meV for the average of samples 2a and 2b. These values are consistent with the values expected from the light hole contribution to the restoring current given by Eq. (6): $E_0 = 43$ meV for sample 1, and $E_0 = 61$ meV for sample 2.

The experimental results for the quantity $j_{p,0}$ are tabulated in Table 1. These values are about 100 times smaller than predicted by Eq. (7), which suggests that the hole capture cross section of the surface Cs states is much smaller than the value expected from the Schottky barrier model with a metallic Cs layer. Also, the parameter $j_{p,0}$ is exponentially dependent on the initial surface band bending V, which varies in the range 0.3–0.5 eV depending on the activation details, adding to the uncertainty.

The observation of the linear dependence of B_N on the NEA value Δ predicted by Eq. (A.7) is strongly supported by the data on the variation of Y with the bias field. Numerical values for B_N were calculated from the sample yield measurements using Eq. (1) and were found to be in the range $0.09 \leqslant B_N \leqslant 0.26$. These values, together with Eq. (A.7) and the value for the optical phonon energy $\hbar\omega_0 = 36$ meV for GaAs, are used to evaluate the electron emission rate $\langle \nu_{\text{emi}} \rangle$ in vacuum. The value of τ_0 in Eq. (A.6) was estimated for GaAs from quantum well magneto-luminescence experiments to be 0.05 ps [23], which gives $\langle \nu_{\text{emi}} \rangle \approx 0.7\,\text{ps}^{-1}$. This value is close to the values found experimentally in the time-resolved electron emission measurements from thin GaAs layers [24].

6. Conclusions

The present experimental results show that the surface escape probability from NEA GaAs surfaces is in the range of $B_N \leqslant 0.26$ and is a linear function of the NEA energy including photovoltage and bias voltage effects. For well activated photocathodes, the quantum yield is observed to increase linearly with the square-root of the bias field. The NEA value Δ is determined from the slope of this dependence giving values of Δ which are similar for all well activated samples.

The time evolution of the photovoltage and the photovoltage dependence on excitation laser intensity have been studied for thin GaAs samples with varying doping concentrations using a long laser pulse technique and a second technique using short pulse lasers in a pump-probe configuration. The results of these measurements show that the photovoltage effect has a strong doping concentration dependence decreasing with increased doping, and diminishing to zero at a doping level of 5×10^{19} cm^{-3}. The experimental determinations of the parameter $j_{p,0}$ are about 1% of the values expected from a Schottky barrier model, indicating that the surface Cs layer has a non-metallic nature.

The overall experimental results are consistent with a model based on electron energy relaxation by multiple phonon emission in the band bending region and tunneling through the surface barrier to vacuum.

Appendix A. Electron kinetics in the BBR: surface escape probability

In this appendix an expression for the surface escape probability B_N is derived. For unstrained GaAs photocathodes the EDC curves are spread over a broad energy band with a width close to the NEA value Δ, implying a long electron stay in the BBR accompanied by energy relaxation. In both bulk and quantum well GaAs structures the most effective mechanism for energy loss is optical phonon emission. One can assume that this mechanism also dominates in the BBR.

In this case the fraction of energy lost in one scattering event is much smaller than Δ. It is then possible to describe the energy relaxation and emission into vacuum by a Fokker–Planck [25,26] type equation for the electron density $n(\epsilon)$ in the BBR at a given energy ϵ:

$$\frac{\partial n(\epsilon)}{\partial t} = -\frac{\partial}{\partial \epsilon}\left[\frac{\epsilon}{\tau_\epsilon}n(\epsilon) - D(\epsilon)\frac{\partial n(\epsilon)}{\partial \epsilon}\right] - v_{\text{emi}}(\epsilon)n(\epsilon)$$
$$= 0, \tag{A.1}$$

where ϵ is the electron energy measured downward from the conduction band edge. The first term in square brackets describes the flow of electrons through the states with energy ϵ due to phonon emission and the second term corresponds to diffusion in energy space. In this equation τ_ϵ is the energy relaxation time, $v_{\text{emi}}(\epsilon)$ is the rate of electron emission into vacuum, and $D(\epsilon)$ is the diffusion coefficient. The emission current density through the energy band $0 \leqslant \epsilon \leqslant \Delta$ can be calculated as

$$j_{\text{emi}} = q \int_0^\Delta v_{\text{emi}}(\epsilon)n(\epsilon)\,d\epsilon. \tag{A.2}$$

To solve Eq. (A.1) we note that the diffusion term, for a broad energy distribution $\Delta \gg kT$ in the electron flow, is of order $kT/\Delta \ll 1$ and can be neglected. Then

Eq. (A.1) reduces to

$$\frac{\partial}{\partial \epsilon}\left[\frac{\epsilon}{\tau_\epsilon}n(\epsilon)\right] = v_{\text{emi}}(\epsilon)n(\epsilon). \tag{A.3}$$

The calculation of the ratio of the emission current through the energy band $0 \leqslant \epsilon \leqslant \Delta$ to the electron flow at $\epsilon = 0$ using Eqs. (A.2) and (A.3) results in

$$B_N = 1 - \exp\left[-\int_0^\Delta \frac{v_{\text{emi}}(\epsilon)\tau_\epsilon(\epsilon)}{\epsilon}\,d\epsilon\right]. \tag{A.4}$$

The rate of electron emission in vacuum is controlled by the transparency of the thin atomic-width barrier at the surface. The transparency is presumably a slowly decreasing function of the electron energy ϵ, and therefore can be replaced in Eq. (A.4) by its average value $\langle v_{\text{emi}}\rangle$. The surface escape probability for the case $B_N \ll 1$ can then be written as

$$B_N = \langle v_{\text{emi}}\rangle\tau_d, \quad \tau_d = \int_0^\Delta \tau_\epsilon\frac{d\epsilon}{\epsilon}. \tag{A.5}$$

For the case where the dominant energy relaxation mechanism is optical phonon emission, the following relation is a valid approximation [26]: [3]

$$\frac{\tau_\epsilon(\epsilon)}{\epsilon} = \frac{\tau_0}{\hbar\omega_0}, \tag{A.6}$$

where $\hbar\omega_0$ is the optical phonon energy and τ_0 is the characteristic time for phonon emission. With these assumptions, τ_d and B_N are linear functions of the NEA value Δ, giving

$$B_N = \frac{\Delta}{E_B}, \quad E_B = \frac{\hbar\omega_0}{\langle v_{\text{emi}}\rangle\tau_0}. \tag{A.7}$$

The linear dependence of the surface escape probability on Δ can be obtained from a more general analysis of electron energy diffusion in the band bending region and does not depend on a surface density of states. This result, the linear dependence of B_N on Δ, is therefore not altered by band bending variations resulting from optical pumping.

---

[3] τ_0 is assumed to be independent of ϵ, a good approximation for the conditions of this experiment.

References

[1] C. Herman, H.-J. Drouhin, G. Lampel, Y. Lassailly, D. Paget, J. Peretti, R. Houdré, F. Ciccacci, H. Riehert, in: C.V. Shank, B.P. Zakharchenya (Eds.), Spectroscopy of Nonequilibrium Electrons and Phonons, Elsevier, 1992, p. 397.

[2] A.V. Subashiev, Yu.A. Mamaev, Yu.P. Yashin, J.E. Clendenin, Phys. Low-Dim. Struct. 1/2 (1999) 1.

[3] A.W. Baum et al., SPIE 2550 (1995) 189.

[4] Yu.A. Mamaev, A.V. Subashiev, Yu.P. Yashin, H.-J. Drouhin, G. Lampel, Solid State Commun. 114 (2000) 401.

[5] A.S. Terekhov, D.A. Orlov, SPIE 2550 (1995) 157.

[6] E.L. Nolle, Fiz. Tverd. Tela 31 (1989) 225, Sov. Phys. Solid State 31 (1989) 196.

[7] H. Tang, in: Proceedings of the Workshop on Photocathodes for Polarized Electron Sources for Accelerators, SLAC-PUB 432 Rev, 1993, p. 344.

[8] M. Woods et al., J. Appl. Phys. 73 (1994) 2295.

[9] B.I. Reznikov, A.V. Subashiev, Semiconductors 32 (1998) 1006, 1309.

[10] K. Togawa et al., Nucl. Instr. Meth. A 414 (1998) 431.

[11] A.S. Jaroshevich et al., in: R.J. Holt, M.A. Miller (Eds.), 7th International Workshop on Polarized Gas Targets and Polarized beams, Urbana, USA, 1997, AIP Conference Proceedings, Vol. 421, 1998, p. 549.

[12] A. Herrera-Gómez, G. Vergara, W.E. Spicer, J. Appl. Phys. 79 (1996) 7318.

[13] M.H. Hecht, Phys. Rev. B 41 (1990) 7918.

[14] A. Bauer, M. Prietsch, S. Molodtsov, C. Laubschat, G. Kaindl, Phys. Rev. B 44 (1991) 4002.

[15] R. Alley et al., Nucl. Instr. Methods A 365 (1995) 1.

[16] Zeroth order design report for the next linear collider, SLAC Report 474, May 1996.

[17] H.C. Casey Jr., M.B. Panish, Heterostructure Lasers, Academic Press, New York, 1978.

[18] J.R. Howorth, A.L. Hammer, E.W. Trawny, Appl. Phys. Lett. 23 (1973) 123.

[19] A.S. Terekhov, D.A. Orlov, A.S. Jaroshevich, G.M. Soldathenko, I.V. Savchenko, L.S. Ronzhin, Fiz. Tverd. Tela 38 (1996) 306, Sov. Phys. Solid State 38 (1996) 171.

[20] E.H. Rhoderick, R.H. Williams, Metal–Semiconductor Contacts, 2nd ed., Clarendon, Oxford, 1988.

[21] QED (now IQE Inc.), 119 Technology Drive, Bethlehem, PA 18015, USA.

[22] B. Schwartz, F. Ermanis, M.H. Brastad, J. Electrochem. Soc. 123 (1976) 1089.

[23] D.N. Mirlin, V.I. Perel', I.I. Reshina, Semiconductors 32 (1998) 770.

[24] J. Schuler et al., Contributed to the Workshop on Polarized Electron Sources and Polarimeters, Nagoya, Japan, 2000. To be published in AIP Conference Proceedings, Proceedings of the 14th International Spin Physics Symposium.

[25] E.M. Lifshitz, L.P. Pitaevskii, Physical Kinetics, Pergamon, London, 1981.

[26] D.N. Mirlin, V.I. Perel', in: C.V. Shank, B.P. Zakharchenya (Eds.), Spectroscopy of Nonequilibrium Electrons and Phonons, Elsevier, 1992, p. 269.